JACS
JOURNAL OF THE AMERICAN CHEMICAL SOCIETY
Communication
pubs.acs.org/JACS

Above Room Temperature Organic Ferroelectrics: Diprotonated 1,4-Diazabicyclo[2.2.2]octane Shifts between Two 2-Chlorobenzoates

Zi-Shuo Yao,[†] Kaoru Yamamoto,[⊥] Hong-Ling Cai,[§] Kazuyuki Takahashi,[‡] and Osamu Sato*[,†]

[†]Institute for Materials Chemistry and Engineering, Kyushu University, 744 Motooka, Nishi-ku, Fukuoka 819-0395, Japan
[⊥]Department of Applied Physics, Okayama University of Science, Okayama 700-0005, Japan
[§]National Laboratory of Solid State Microstructures and School of Physics, Nanjing University, Nanjing 210093, P.R. China
[‡]Department of Chemistry, Graduate School of Science, Kobe University, Kobe 657-8501, Hyogo, Japan

Supporting Information

ABSTRACT: A pure organic single crystal, $[H_2dabco]\cdot[2CB]_2$ ($[H_2dabco]^{2+}$ = diprotonated 1,4-diazabicyclo-[2.2.2]octane, $2CB^-$ = 2-chlorobenzoate), which undergoes a ferroelectric-to-paraelectric phase transition above room temperature (~323 K upon heating), was prepared and characterized. This ferroelectric crystal possesses a distinctive supramolecular architecture composed of discrete H-bonded trimeric units (two $2CB^-$ anions bridged by one $[H_2dabco]^{2+}$ cation through N−H···O hydrogen bond interactions). In the paraelectric phase, the $[H_2dabco]^{2+}$ cation is rotationally disordered and lies at the symmetric center of the trimer. Upon cooling, it is frozen in an ordered state and deviates toward a $2CB^-$ anion at one end along the H-bond. The collective displacement of the cations leads to a polarization of the single crystal along the crystallographic *c* axis, which is confirmed by the temperature dependence of the second harmonic generation and spontaneous polarization. A significant increase in the phase transition temperature of the deuterated analogue suggests that the proton plays an important role in the ferroelectric phase transition.

The development of molecular-based organic ferroelectrics has attracted increasing attention due to their mechanical flexibility, environmental friendliness, and potential applications in organic devices.[1,2] According to their structural characteristics, pure organic ferroelectrics are generally classified into $\pi\cdots\pi$ stacked electron donor−acceptor systems and H-bonded supramolecular aggregates. In the latter, H-bond interactions play important roles in securing the supramolecular structure and affecting the ferroelectric behavior of the materials.[3]

In typical H-bonded supramolecular ferroelectrics, the polar components can be switched along H-bonds, resulting in the reversal of spontaneous polarization.[4] Moreover, several sophisticated organic ferroelectrics with extended one-dimensional or three-dimensional structures linked by H-bond interactions have been developed;[4b,5] some of these have demonstrated remarkable ferroelectric performance. However, achieving ferroelectricity in an organic solid built from discrete H-bonded molecular assemblies still remains an extraordinary challenge.[6] Ferroelectrics with such structures are not only interesting for the enrichment of the family of organic ferroelectrics but also potentially significant for mitigating the detrimental size effect that is usually suffered by ferroelectrics with extended structures.[7] In this study, we attempted to prepare an organic ferroelectric constructed from H-bonded trimeric units, where the function of the H-bonds was restricted within the trimeric unit region. The trimeric structure represents one of the simplest structural modes for ferroelectrics, wherein the middle component can shift between two end molecules along the H-bonds, influencing the spontaneous polarization of the bulk material.

After investigating a variety of compounds,[8] we found that $[H_2dabco]\cdot[2CB]_2$ (**1**), a supramolecular architecture constructed from trimeric units, underwent a phase transition from a ferroelectric phase at room temperature (rt) to a paraelectric phase at higher temperature. In the crystal of **1**, the strong H-bond interactions were constrained within the trimeric unit. During the paraelectric-to-ferroelectric phase transition, the $[H_2dabco]^{2+}$ cation in the middle position deviated from the inversion center, accompanied by a disorder-to-order structural transition, leading to a spontaneous polarization of the single crystal.

Single crystals of **1** were grown via slow evaporation of a methanol or acetone solution containing 2-chlorobenzoic acid (2CBA) and 1,4-diazabicyclo[2.2.2]octane (dabco) in a molar ratio of 2:1 at constant rt. At or below rt (referred to as low temperature, LT), **1** crystallized in polar space group $Pca2_1$, belonging to the orthorhombic crystal system. The asymmetric unit contained one integral trimeric unit in which two acid molecules were bridged by one dabco molecule with N···O hydrogen bond lengths of 2.555(2) and 2.593(2) Å, respectively (Figure 1b). The remarkably short N···O distances suggested strong intermolecular H-bond interactions. The planes of the two 2CB anions at either end were slightly twisted with respect to each other at a small dihedral angle of 7.98(6)° (Figure S2). The linear trimers, which formed small included angles with the crystallographic (001) face, were arranged in a herringbone pattern in the *ab* plane (Figure S3). In the crystal, the H-bond interactions were virtually constrained within the trimeric unit, although the very weak C−H···O, C−H···Cl, C−H···π, and C−Cl···Cl−C intermolecular interactions assisted in anchoring the structure (Figures S5 and S6, Table S3). As shown in Figure S7,

Received: April 12, 2016
Published: August 31, 2016

DOI: 10.1021/jacs.6b03747
J. Am. Chem. Soc. 2016, 138, 12005−12008

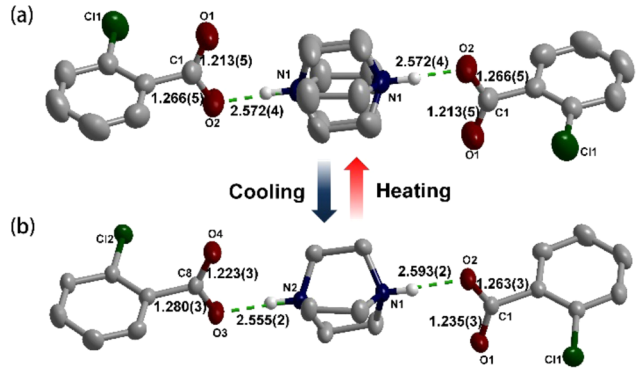

Figure 1. Trimeric unit at different temperatures. (a) The high-temperature phase (338 K). The $[H_2dabco]^{2+}$ cation is heavily disordered and located at the symmetry center of the trimer. (b) The low-temperature phase (223 K). The cation is frozen in an ordered state and shifts toward a 2CB anion at one end, as indicated by the differential in the N···O distances. The green dotted lines indicate the intermolecular N−H···O hydrogen bonds. The thermal ellipsoids are drawn at a 50% probability level. Atoms: N, blue; C, gray; O, red; Cl, green. The H-atoms on the C-atoms are omitted for clarity.

the two acidic protons revealed from the differential Fourier map were close to the dabco molecule, which is consistent with the short C−O single bond lengths identified from the single-crystal structure (1.263(3) Å for C1−O2 and 1.280(3) Å for C8−O3).[9] The migration of protons from the O atom side of the organic acid to the N atom side of the dabco was further supported by the IR spectra (Figure S8). Compared with 2CBA, the C═O stretching vibration absorption band shifted from 1670 to 1650 cm^{-1} in **1**, and the peak associated with C−O vibrations increased from 1316 to 1376 cm^{-1}, indicating the transfer of protons from O to N atoms in the cocrystal.[10] It should be noted that the crystal structure at rt was first reported by Skovsgaard et al.[8b]

Differential scanning calorimetry (DSC) analysis revealed that **1** underwent a phase transition upon heating above rt (~323 K), and the corresponding exothermic peak in the cooling mode was observed at ~320 K (Figure 2a). The broad anomaly peak and the small hysteresis loop (~3 K) indicated that a second-order phase transition occurred.

To elucidate the crystal structure of the high-temperature (HT) phase, single-crystal analysis was performed at 338 K (Figure 1a). It was found that at the HT phase, the space group of **1** changed to *Pbca*, a nonpolar space group that also belongs to the orthorhombic system. Correspondingly, the four symmetric

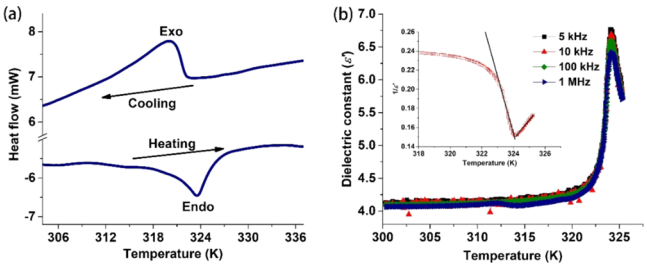

Figure 2. DSC and dielectric constant (ε') of **1**. (a) DSC curve of **1**. Exo, exothermic peak; Endo, endothermic peak. (b) Temperature dependence of the real parts of the dielectric constant of **1** along the crystallographic *c* direction. The inset of (b) shows a linear fit to the Curie−Weiss law at a frequency of 100 kHz.

elements (E, C_2, σ_v, and σ_d) of **1** in the LT phase were doubled to eight (E, $3C_2$, i, σ_v, σ_d, and σ_h) for the HT phase, which was in good agreement with a ferroelectric-to-paraelectric phase transition with the Aizu notation *mmm*F*mm*2.[1b,11] Notably, the space group of the ferroelectric phase ($Pca2_1$) falls into a subgroup of the paraelectric space group (*Pbca*), which is in agreement with the Curie symmetry principle (Figure S10). In the HT phase, the asymmetric unit contained a half trimer unit; the $[H_2dabco]^{2+}$ cation was rotationally disordered around its N···N axis and lay in the center of inversion (Figure S4). Consequently, the different N···O distances in the LT phase became equal (2.572(4) Å), and the planes of the two 2CB anions at either end became parallel to each other (Figures 1a and S2). The short C−O single bond length (1.266(5) Å) was maintained, and the IR peaks corresponding to the C−O vibrations remained nearly unchanged during the heating process, which suggested that no proton transfer occurred during the phase transition (Figure S9).

The structural transformation was further investigated using variable temperature powder X-ray diffraction (PXRD). A comparison of PXRD patterns obtained at different temperatures revealed that the phase transition occurred above 323 K upon heating (Figure S12). The diffraction patterns fit well with those in the simulated patterns for related phases, confirming the structure and phase purity (Figure S11).

The temperature dependence of the dielectric constant (ε') was evaluated for single-crystal samples with the applied electric field parallel to the crystallographic *c* axis. As shown in Figure 2b, **1** exhibited a sharp peak with a maximum at ~324 K, which is consistent with the DSC and PXRD results. The sharp ε' peak at the phase transition temperature (T_c) is a typical characteristic of ferroelectric transitions. In the vicinity of T_c, ε' obeyed the Curie−Weiss law, $\varepsilon' = C_{ferro}/(T_0 - T)$ ($T < T_c$) or $\varepsilon' = C_{para}/(T - T_{0'})$ ($T > T_c$). A fit of the reciprocal dielectric constant ($1/\varepsilon'$) vs T plot afforded C_{ferro} = 16.8 K and C_{para} = 49.4 K. The ratio of C_{para}/C_{ferro} = 2.9, was in agreement with the character of a second order phase transition. Compared to previous reported pure organic ferroelectrics, the magnitude of the peak value of ε' (~6.5) and the Curie constant were much smaller, suggesting a weak spontaneous polarization of **1**.[6] The dielectric constant of **1** was highly anisotropic (Figure S13). At the phase transition temperature, the dielectric anomalies along the *a* and *b* axes were negligible in comparison to that along the *c* axis, suggesting that the spontaneous polarization occurred along the crystallographic *c* axis.

Analysis of second harmonic generation (SHG) is a sensitive method for probing the existence of ferroelectric domains and symmetry breaking from centrosymmetric to noncentrosymmetric structures during phase transitions.[5b,e,12] As shown in Figure 3a, the temperature dependence of the SHG intensity gradually decreased upon heating of **1** and finally reached zero at 325 K. The disappearance of the bright spot above T_c confirmed the emergence of inversion symmetry at the HT phase, which was in good agreement with the results of the single-crystal structure analyses (insets of Figure 3a).[12a] In addition, the gradual change in SHG intensity of **1** in the vicinity of the T_c further verified the second-order nature of the phase transition (also see Video S1).

To further demonstrate the ferroelectric properties of **1**, the temperature dependence of the spontaneous polarization obtained from the integration of the pyroelectric current was investigated under a reverse electric field. As shown in Figure 3b, the spontaneous polarization can be reversed by a DC electric

DOI: 10.1021/jacs.6b03747
J. Am. Chem. Soc. 2016, 138, 12005−12008

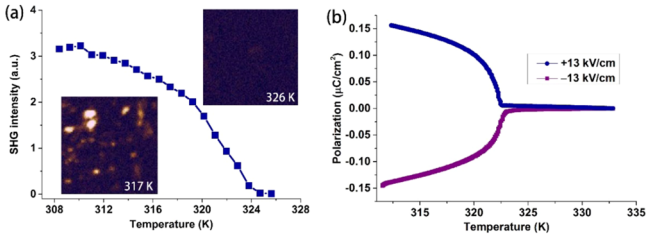

Figure 3. Temperature dependence of the SHG effect (a) and spontaneous polarization (b) of **1**. The insets of (a) show the SHG signal pictures at 326 (top right) and 317 K (bottom left); the bright spots observed below the phase transition temperature confirm the noncentrosymmetric structure at the LT phase. Spontaneous polarization was determined from the integration of pyroelectric current.

field, definitively confirming the ferroelectricity of the crystal below the phase transition point. The gradual decrease in spontaneous polarization in the heating stage was consistent with the continuous character of the ferroelectric phase transition. Notably, the spontaneous polarization obtained from integration of the pyroelectric current ($P_s \approx 0.16\ \mu C/cm^2$) is consistent with the value obtained from the DFT calculation: $P_s = \mu_{sc}N \approx 0.18\ \mu C/cm^2$, where $\mu_{sc} = 8.83 \times 10^{-31}$ C·m is the dipole moment of the trimeric unit along the crystallographic *c* axis (Figure S14); $N = Z/V_{cell} = 1.99 \times 10^{27}\ m^{-3}$ is the number of trimeric units per cubic meter. We have not been able to observe ferroelectric hysteresis loops for the crystal, perhaps due to the low mobility of the domain wall, as in the case of another atypical organic ferroelectric single crystal whose structure was connected via non-H-bond interactions.[13]

To clarify the microscopic origin of the ferroelectric–paraelectric phase transition, the structural transformation was further investigated. At the HT phase, the $[H_2dabco]^{2+}$ cations exhibited structural disordered and located at the symmetry center of trimers, corresponding to a paraelectric phase. At temperatures below the phase transition point, it was found that the $[H_2dabco]^{2+}$ cations were frozen so as to be ordered and shifted to one of the two energetically equivalent positions around the center of trimer along the H-bond. Consequently, two N···O hydrogen bonds with different distance were detected in the LT phase ($\Delta d_{N\cdots O} = 0.038$ Å) (Figure 1). The change in the trimer unit disrupted the crystal symmetry and led to the loss of the crystallographic symmetric center. The displacement directions for $[H_2dabco]^{2+}$ from the HT symmetric positions are indicated by the blue arrows in Figure 4. According to the symmetry operations of the space group $Pca2_1$, a spontaneous polarization of the bulk single crystal emerged along the crystallographic *c* direction (denoted by the green arrow in Figure 4), while the components along the crystallographic *a* and *b* directions canceled out because of the existence of glide planes.

The entropy change, ΔS, of the phase transition was estimated to be 2.35 $J\cdot mol^{-1}\cdot K^{-1}$ from DSC measurements. According to $\Delta S = R \ln W$ ($R = 8.31\ J\cdot mol^{-1}\cdot K^{-1}$ is the gas constant, and W stands for the ratio of respective microscopic states), we calculated the value of $W = 1.33$, which is smaller than 2, suggesting that the transition was more complex than a simple 2-fold order–disorder model. During the phase transition, the C–H···O hydrogen bond interactions between $[H_2dabco]^{2+}$ cation and $2CB^-$ anions from neighboring trimers underwent a substantial variation (Figure S6), suggesting that the weak molecular interactions between trimers are important for the order–disorder phase transition of the $[H_2dabco]^{2+}$ cations.[14] Notably, the rotational disorder of dabco molecules in halogen-

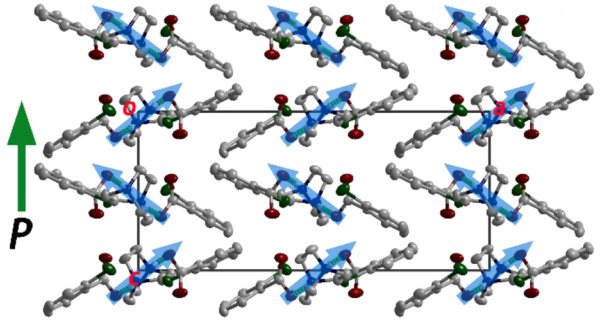

Figure 4. Schematic diagram of the appearance of the spontaneous polarization. Molecular packing viewed along the crystallographic *b* direction. The blue arrows illuminate the directions of $[H_2dabco]^{2+}$ displacement at the LT phase from the center position of the trimer. The green arrow denotes the spontaneous polarization. Atoms: N, blue; C, gray; O, red; Cl, green. The H-atoms on the C-atoms are omitted for clarity.

bonded trimeric units has been reported in two-component amphidynamic cocrystals very recently.[15]

Moreover, the H-bond interactions within the trimer also perform an important function in the phase transition. As mentioned above, the protons persisted in bonding to the dabco during the ferroelectric phase transition, which was akin to the situation reported for Phz-H_2xa (Phz = phenazine, H_2xa = 2,5-dihalo-3,6-dihydroxy-*p*-benzoquinones), for which incipient proton transfer induces molecular displacive motion and consequently generates spontaneous polarization.[5a,16] This proton displacement is attributed to the well-matched proton affinities of Phz ($pK_a = 1.20$) and H_2xa ($pK_{a1} = 0.73$–0.80).[2b] For **1**, $[H_2dabco]^{2+}$ and 2CBA have nearly the same acidic dissociation constants ($pK_{a2} = 2.97$ for $[H_2dabco]^{2+}$ and $pK_a = 2.92$ for 2CBA, see Scheme 1),[17] strongly suggesting that the

Scheme 1. Acidic Dissociation Constants of Related Compounds

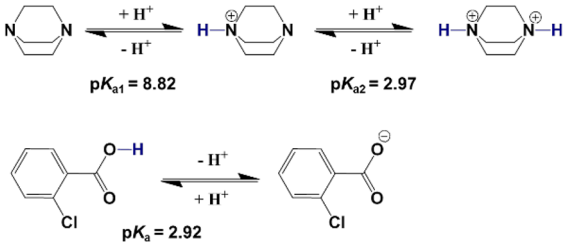

$[H_2dabco]^{2+}$ displacement is possibly induced by the incipient proton transfer involved with the order–disorder structural transition. One typical feature of proton-transfer-induced ferroelectricity is that deuteration has a significant effect on the T_c.[2a,18] Hence, the deuterated analogue **2** was synthesized and characterized to investigate this deuteration effect. As can be seen in Figure S15, the T_c was substantially elevated by replacing the acidic H with D; i.e., the T_c of **2** was ~12 K higher than that of **1**. The significant elevation of T_c confirmed that acidic protons play a crucial role in the cation displacement, consistent with the mechanism of incipient proton transfer accompanying an order–disorder phase transition.

In conclusion, we demonstrate here an organic ferroelectric with distinctive structural architecture that was built from discrete H-bonded molecular assemblies. The above room temperature ferroelectricity stems from displacive motion of the

DOI: 10.1021/jacs.6b03747
J. Am. Chem. Soc. 2016, 138, 12005–12008

middle cation between two end molecular anions accompanied by an order−disorder structural change. The large shift in the phase transition temperature upon deuteration manifests the importance of the H-bond in the ferroelectricity, although the weak molecular interactions between the trimers cannot be neglected in the present study. Understanding the origin of the spontaneous polarization in this unique structure will be useful for the development of molecular-based ferroelectrics with enhanced functional properties for use in microdevices.

■ ASSOCIATED CONTENT

Supporting Information

The Supporting Information is available free of charge on the ACS Publications website at DOI: 10.1021/jacs.6b03747.

Experimental details, PXRD and IR spectra, and structures, including Figures S1−S16 and Tables S1−S4 (PDF)

X-ray crystallographic data for 1 at 223 K, 1 at 293 K, 1 at 338 K, 2 at 298 K, and 2 at 343 K (CIF)

Video S1, showing the gradual change in SHG intensity of **1** in the vicinity of the T_c (MPG)

■ AUTHOR INFORMATION

Corresponding Author

*sato@cm.kyushu-u.ac.jp

Notes

The authors declare no competing financial interest.

■ ACKNOWLEDGMENTS

This work was partly supported by JSPS KAKENHI Grant No. 16H00843 and the MEXT Projects of "Integrated Research Consortium on Chemical Sciences". Z.-S.Y. was partially supported by China Scholarship Council Scholarship

■ REFERENCES

(1) (a) Lines, M. E.; Glass, A. M. *Principles and Applications of Ferroelectrics and Related Materials*; Clarendon Press: Oxford, UK, 1977. (b) Zhang, W.; Xiong, R. G. *Chem. Rev.* **2012**, *112*, 1163. (c) Katrusiak, A.; Szafrański, M. *Phys. Rev. Lett.* **1999**, *82*, 576. (d) Jakubas, R.; Krzewska, U.; Bator, G.; Sobczyk, L. *Ferroelectrics* **1988**, *77*, 129. (e) Xu, G.-C.; Ma, X.-M.; Zhang, L.; Wang, Z.-M.; Gao, S. *J. Am. Chem. Soc.* **2010**, *132*, 9588. (f) Jain, P.; Ramachandran, V.; Clark, R. J.; Zhou, H. D.; Toby, B. H.; Dalal, N. S.; Kroto, H. W.; Cheetham, A. K. *J. Am. Chem. Soc.* **2009**, *131*, 13625. (g) Zhou, B.; Kobayashi, A.; Cui, H.-B.; Long, L.-S.; Fujimori, H.; Kobayashi, H. *J. Am. Chem. Soc.* **2011**, *133*, 5736.

(2) (a) Horiuchi, S.; Kumai, R.; Tokura, Y. *Angew. Chem., Int. Ed.* **2007**, *46*, 3497. (b) Horiuchi, S.; Tokura, Y. *Nat. Mater.* **2008**, *7*, 357. (c) Akutagawa, T.; Koshinaka, H.; Sato, D.; Takeda, S.; Noro, S.-I.; Takahashi, H.; Kumai, R.; Tokura, Y.; Nakamura, T. *Nat. Mater.* **2009**, *8*, 342. (d) Kobayashi, K.; Horiuchi, S.; Kumai, R.; Kagawa, F.; Murakami, Y.; Tokura, Y. *Phys. Rev. Lett.* **2012**, *108*, 237601. (e) Tayi, A. S.; Kaeser, A.; Matsumoto, M.; Aida, T.; Stupp, S. I. *Nat. Chem.* **2015**, *7*, 281. (f) Fu, D. W.; Cai, H. L.; Liu, Y. M.; Ye, Q.; Zhang, W.; Zhang, Y.; Chen, X. Y.; Giovannetti, G.; Capone, M.; Li, J. Y.; Xiong, R. G. *Science* **2013**, *339*, 425.

(3) Jeffrey, G. A. *An Introduction to Hydrogen Bonding*; Oxford University Press: Oxford, UK, 1997.

(4) (a) Fujioka, J.; Horiuchi, S.; Kagawa, F.; Tokura, Y. *Phys. Rev. Lett.* **2009**, *102*, 197601. (b) Horiuchi, S.; Kagawa, F.; Hatahara, K.; Kobayashi, K.; Kumai, R.; Murakami, Y.; Tokura, Y. *Nat. Commun.* **2012**, *3*, 1308.

(5) (a) Horiuchi, S.; Ishii, F.; Kumai, R.; Okimoto, Y.; Tachibana, H.; Nagaosa, N.; Tokura, Y. *Nat. Mater.* **2005**, *4*, 163. (b) Horiuchi, S.; Tokunaga, Y.; Giovannetti, G.; Picozzi, S.; Itoh, H.; Shimano, R.; Kumai, R.; Tokura, Y. *Nature* **2010**, *463*, 789. (c) Sun, Z.; Chen, T.; Luo, J.; Hong, M. *Angew. Chem., Int. Ed.* **2012**, *51*, 3871. (d) Szafrański, M. *Angew. Chem., Int. Ed.* **2013**, *52*, 7076. (e) Ye, H. Y.; Zhang, Y.; Noro, S.; Kubo, K.; Yoshitake, M.; Liu, Z. Q.; Cai, H. L.; Fu, D. W.; Yoshikawa, H.; Awaga, K.; Xiong, R. G.; Nakamura, T. *Sci. Rep.* **2013**, *3*, 2249. (f) Horiuchi, S.; Kumai, R.; Tokura, Y. *Adv. Mater.* **2011**, *23*, 2098. (g) Horiuchi, S.; Kumai, R.; Tokura, Y. *J. Am. Chem. Soc.* **2013**, *135*, 4492.

(6) Horiuchi, S.; Kumai, R.; Tokunaga, Y.; Tokura, Y. *J. Am. Chem. Soc.* **2008**, *130*, 13382.

(7) (a) Polking, M. J.; Han, M.-G.; Yourdkhani, A.; Petkov, V.; Kisielowski, C. F.; Volkov, V. V.; Zhu, Y.; Caruntu, G.; Paul Alivisatos, A.; Ramesh, R. *Nat. Mater.* **2012**, *11*, 700. (b) Hu, Z.; Tian, M.; Nysten, B.; Jonas, A. M. *Nat. Mater.* **2009**, *8*, 62. (c) Ray, S.; Kolen'ko, Y. V.; Fu, D.; Gallage, R.; Sakamoto, N.; Watanabe, T.; Yoshimura, M.; Itoh, M. *Small* **2006**, *2*, 1427. (d) Miyajima, D.; Araoka, F.; Takezoe, H.; Kim, J.; Kato, K.; Takata, M.; Aida, T. *Science* **2012**, *336*, 209.

(8) (a) Yao, Z.-S.; Sato, O. *Acta Crystallogr., Sect. E* **2014**, *70*, o154. (b) Skovsgaard, S.; Bond, A. D. *Acta Crystallogr., Sect. E* **2008**, *64*, o1416.

(9) (a) Ueda, A.; Yamada, S.; Isono, T.; Kamo, H.; Nakao, A.; Kumai, R.; Nakao, H.; Murakami, Y.; Yamamoto, K.; Nishio, Y.; Mori, H. *J. Am. Chem. Soc.* **2014**, *136*, 12184. (b) Skovsgaard, S.; Bond, A. D. *CrystEngComm* **2009**, *11*, 444.

(10) Sundaraganesan, N.; Joshua, B. D.; Radjakoumar, T. *Indian J. Pure Appl. Phys.* **2009**, *47*, 248.

(11) (a) Aizu, K. *J. Phys. Soc. Jpn.* **1969**, *27*, 387. (b) Hang, T.; Zhang, W.; Ye, H.-Y.; Xiong, R.-G. *Chem. Soc. Rev.* **2011**, *40*, 3577.

(12) (a) Yamamoto, K.; Kowalska, A. A.; Yakushi, K. *Appl. Phys. Lett.* **2010**, *96*, 122901. (b) Yamamoto, K.; Iwai, S.; Boyko, S.; Kashiwazaki, A.; Hiramatsu, F.; Okabe, C.; Nishi, N.; Yakushi, K. *J. Phys. Soc. Jpn.* **2008**, *77*, 074709. (c) Cai, H.-L.; Zhang, W.; Ge, J.-Z.; Zhang, Y.; Awaga, K.; Nakamura, T.; Xiong, R.-G. *Phys. Rev. Lett.* **2011**, *107*, 147601.

(13) Bordeaux, D.; Bornarel, J.; Capiomont, A.; Lajzerowicz-Bonneteau, J.; Lajzerowicz, J.; Legrand, J. F. *Phys. Rev. Lett.* **1973**, *31*, 314.

(14) (a) Lemouchi, C.; Vogelsberg, C. S.; Zorina, L.; Simonov, S.; Batail, P.; Brown, S.; Garcia-Garibay, M. A. *J. Am. Chem. Soc.* **2011**, *133*, 6371. (b) Lemouchi, C.; Yamamoto, H. M.; Kato, R.; Simonov, S.; Zorina, L.; Rodríguez-Fortea, A.; Canadell, E.; Wzietek, P.; Iliopoulos, K.; Gindre, D.; Chrysos, M.; Batail, P. *Cryst. Growth Des.* **2014**, *14*, 3375.

(15) Catalano, L.; Pérez-Estrada, S.; Terraneo, G.; Pilati, T.; Resnati, G.; Metrangolo, P.; Garcia-Garibay, M. A. *J. Am. Chem. Soc.* **2015**, *137*, 15386.

(16) Kumai, R.; Horiuchi, S.; Sagayama, H.; Arima, T.-h.; Watanabe, M.; Noda, Y.; Tokura, Y. *J. Am. Chem. Soc.* **2007**, *129*, 12920.

(17) (a) Guzonas, D. A.; Irish, D. E. *Can. J. Chem.* **1988**, *66*, 1249. (b) Dixon, S. L.; Jurs, P. C. *J. Comput. Chem.* **1993**, *14*, 1460.

(18) Horiuchi, S.; Kumai, R.; Tokura, Y. *J. Am. Chem. Soc.* **2005**, *127*, 5010.

DOI: 10.1021/jacs.6b03747
J. Am. Chem. Soc. 2016, 138, 12005−12008